FEBS Letters 587 (2013) 2691–2697

FEBS Letters

journal homepage: www.FEBSLetters.org

Complete subsite mapping of a "loopful" GH19 chitinase from rye seeds based on its crystal structure

Takayuki Ohnuma [a], Naoyuki Umemoto [a], Kaori Kondo [a], Tomoyuki Numata [b,*], Tamo Fukamizo [a,*]

[a] Department of Advanced Bioscience, Kinki University, 3327–204 Nakamachi, Nara 631-8505, Japan
[b] Biomedical Research Institute, National Institute of Advanced Industrial Science andTechnology (AIST), 1-1-1 Higashi, Tsukuba 305-8566, Japan

ARTICLE INFO

Article history:
Received 30 May 2013
Revised 1 July 2013
Accepted 1 July 2013
Available online 18 July 2013

Edited by Richard Cogdell

Keywords:
Crystal structure
GH19 chitinase
Rye seed
Chitin oligosaccharide
Domain motion

ABSTRACT

Crystallographic analysis of a mutated form of "loopful" GH19 chitinase from rye seeds a double mutant RSC-c, in which Glu67 and Trp72 are mutated to glutamine and alanine, respectively, (RSC-c-E67Q/W72A) in complex with chitin tetrasaccharide $(GlcNAc)_4$ revealed that the entire substrate-binding cleft was completely occupied with the sugar residues of two $(GlcNAc)_4$ molecules. One $(GlcNAc)_4$ molecule bound to subsites −4 to −1, while the other bound to subsites +1 to +4. Comparisons of the main chain conformation between liganded RSC-c-E67Q/W72A and unliganded wild type RSC-c suggested domain motion essential for catalysis. This is the first report on the complete subsite mapping of GH19 chitinase.
© 2013 Federation of European Biochemical Societies. Published by Elsevier B.V. All rights reserved.

1. Introduction

Chitinases (EC 3.2.1.14) hydrolyze β-1,4-glycosidic linkages of chitin, and have been classified into families GH18 and GH19 according to the CAZy database (http://www.cazy.org/) [1]. Although GH18 chitinases are widely distributed in living organisms from bacteria to humans [2–6], GH19 enzymes are only found in plants and some bacteria [7]. Plants constitutively or inducibly produce various types of GH18 and GH19 chitinases [8]. Among the plant chitinases, the first crystal structure was reported for a family GH19 chitinase from barley seeds [9]. The barley enzyme is composed of two lobes, both of which are rich in α-helical structures. Five loop structures (Loops I–V) are located at both ends of the substrate-binding groove lying in between the two lobes ("loopful" chitinases). Crystal structure of another "loopful" chitinase was reported for a GH19 enzyme isolated from papaya latex [10]. On the other hand, a GH19 chitinase lacking the loops except Loop III ("loopless" chitinases) was isolated from moss, *Bryum coronatum* [11]. Based on the amino acid sequence alignment, the structure of the moss enzyme is closely related to those of GH19 chitinases from *Streptomyces griseus* HUT6037 [12], *Streptomyces coelicolor* A3(2) [13], and Norway spruce [14]. Thus, the structural organization of the GH19 enzymes was intensively studied, and the structural data have been accumulated. However, their mechanisms of action are not fully understood, due to a lack of information on the enzyme–substrate complex. It is highly desirable to analyze the binding mode of chitin oligosaccharides, $(GlcNAc)_n$, to the plant GH19 chitinases.

The binding mode of $(GlcNAc)_n$ to the GH19 enzymes was investigated using kinetic analysis of the HPLC-based time-course of the $(GlcNAc)_n$ degradation [15,16]. This analysis revealed that the substrate-binding cleft of GH19 chitinases from rice and barley seeds consists of sixsubsites, −3 to +3, based on the subsite nomenclature proposed by Davies et al. [17]. However, $(GlcNAc)_6$ was used as the substrate in the kinetic analysis. Therefore, the substrate-binding cleft might not be fully occupied with the substrate, and analysis using $(GlcNAc)_6$ is unlikely to provide information on the entire substrate-binding cleft. Recently, we successfully analyzed the crystal structure of a "loopful" GH19 chitinase from rye seeds (RSC-c) in complex with $(GlcNAc)_4$ [18], and revealed that the tetramer binds to positively numbered subsites,+1 to +4,

Abbreviations: GlcNAc, 2-acetamido-2-deoxy-β-D-glucopyranose; $(GlcNAc)_n$, β-1,4-linked oligosaccharide of GlcNAc with a polymerization degree of n; RSC-c, wild type GH19 chitinase from rye seeds; RSC-c-E67Q/W72A, a double mutant RSC-c, in which Glu67 and Trp72 are mutated to glutamine and alanine, respectively; 2 × $(GlcNAc)_4$, two molecules of $(GlcNAc)_4$; MD, molecular dynamics

* Corresponding authors. Fax: +81 29 861 6773 (T. Numata), +81 742 43 8976 (T. Fukamizo).
E-mail addresses: t-numata@aist.go.jp (T. Numata), fukamizo@nara.kindai.ac.jp (T. Fukamizo).

0014-5793/$36.00 © 2013 Federation of European Biochemical Societies. Published by Elsevier B.V. All rights reserved.
http://dx.doi.org/10.1016/j.febslet.2013.07.008

and that Trp72 is involved in the interaction with the +4 GlcNAc. The substrate-binding cleft of the "loopful" GH19 chitinase is likely to be more extended than expected from the kinetic analysis of the HPLC-based reaction time-courses [15,16]. However, no information has been obtained for the negatively numbered subsites of the "loopful" GH19 enzymes. Here, we mutate Trp72 of RSC-c to alanine to facilitate the oligosaccharide binding to the negatively numbered subsites, and the catalytic residue Glu67 is also mutated to glutamine to exclude hydrolytic effect (RSC-c-E67Q/W72A). Using the double mutant of RSC-c, we solve the crystal structure of the mutant enzyme in complex with $(GlcNAc)_4$.

2. Materials and methods

2.1. Production of the double mutant, RSC-c-E67Q/W72A

The double mutant RSC-c-E67Q/W72A gene was obtained by site-directed mutagenesis of the E67Q mutant gene previously obtained [19] using a QuikChange site-directed mutagenesis kit (Stratagene). The oligonucleotides used to introduce the second mutation were 5′-AGACCACCGGCGGGGCGGCGACCGCA-3′ and 5′-TGCGGTCGCCGCCCCGCCGGTGGTCT-3′ (the mutation site is underlined). Prior to expression of the mutant enzyme, the entire coding region of the mutant was sequenced to verify the presence of the desired mutations and absence of unintended mutations. The double mutant RSC-c-E67Q/W72A was successfully produced and purified by the methods developed for the wild type enzyme [19].

2.2. Crystallization and data collection

Crystallization conditions were screened using the sparse-matrix sampling method by sitting drop vapor diffusion at 20 °C. Under optimized crystallization conditions, 1 μl of protein solution (5 mg/ml in water) containing 9.5 mM $(GlcNAc)_4$ (Seikagaku Biobusiness Co., Tokyo) was mixed with 1 μl of reservoir solution containing 0.1 M NaCl, 0.1 M HEPES (pH 7.5), and 1.6 M $(NH_4)_2SO_4$. Octahedral crystals grew within 2 weeks. For data collection, the crystals were transferred into the cryoprotectant solution containing 0.1 M NaCl, 0.1 M HEPES (pH 7.5), and 1.6 M $(NH_4)_2SO_4$, and 20% ethylene glycol, and then flash-cooled in a nitrogen stream at 95 K. Diffraction data were collected at the beam-line BL-17A of the Photon Factory (Ibaraki, Japan) using an ADSC Q270 CCD detector at a cryogenic temperature (95 K). Data were integrated and scaled with HKL2000 [20]. Processing statistics are summarized in Table 1.

2.3. Structural determination and refinement

The structure of RSC-c-E67Q/W72A was first solved by the molecular replacement method using the program MOLREP [21], in which the structure of unliganded RSC-c, PDB code 4DWX [18], served as a search model. One protein molecule was located in the crystallographic asymmetric unit. The model was improved by several rounds of refinement with REFMAC5 [22] and manual rebuilding with COOT [23]. The structure of RSC-c-E67Q/W72A was refined to an R_{work}/R_{free} of 0.182/0.207 at a resolution of 1.9 Å. The final model contains one protein molecule that includes residues 1–243, two $(GlcNAc)_4$ molecules, one ethylene glycol, five sulfate ions, and 187 water molecules. The stereochemistry of the model was verified using PROCHECK [24], showing 88.9%, 10.6%, 0.0%, and 0.5% of protein residues in the most favored, additionally allowed, generously allowed, and disallowed regions of the Ramachandran plot, respectively. The residue (0.5%), His121 in the protein, lies in the disallowed region of the Ramachandran plot; however, this residue fits well in the electron density map. His121 is located on a loop and contributes to filling the space of the molecule. Molecular graphics were illustrated with PyMol software (http://www.pymol.org/). Refinement statistics are summarized in Table 1.

Table 1
Summary of data collection and refinement statistics.

Data collection	
Space group	$P4_32_12$
Cell dimensions	
a, *b*, *c* (Å)	78.8, 78.8, 95.1
α, β, γ (°)	90, 90, 90
Wavelength (Å)	0.98
Resolution (Å)	50–1.90 (1.93–1.90)
R_{merge}[a]	0.104 (0.332)
R_{meas}[b]	0.107
R_{pim}[b]	0.029
$I/\sigma I$	44.8 (11.0)
Completeness (%)	100 (100)
Redundancy	14.2 (14.5)
Wilson B factor (Å^2)	16.1
Refinement	
Resolution (Å)	50–1.90
No. of reflections	22984
R_{work}[c]/R_{free}[d]	0.182/0.207
No. of atoms	
Protein	1834
Ligand/ion	143
Water	187
Average B-factors (Å^2)	
Protein	12.8
Ligand/ion	18.1
Water	23.1
RMS deviations	
Bond lengths (Å)	0.007
Bond angles (°)	1.1

The numbers in parentheses are for the last shell.
[a] $R_{merge} = \Sigma|I_{avg} - I_i|/\Sigma I_i$.
[b] Definitions of R_{meas} and R_{pim} can be found in Weiss.
[c] $R_{work} = \Sigma|F_o - F_c|/\Sigma F_o$ for reflections of working set.
[d] $R_{free} = \Sigma|F_o - F_c|/\Sigma F_o$ for reflections of test set (5.0% of total reflections).

2.4. Protein data bank entry

The atomic coordinates and structural factors were deposited in the Protein Data Bank under the accession code 4J0L.

3. Results and discussion

3.1. Overall structure of liganded RSC-c-E67Q/W72A

In the crystal structure of RSC-c-E67Q/W72A in complex with $(GlcNAc)_4$, we observed clear electron density for two molecules of $(GlcNAc)_4$, $2 \times (GlcNAc)_4$, within the substrate-binding cleft, in which their sugar residues completely occupied the entire region of the substrate-binding cleft (Fig. 1). One of the $(GlcNAc)_4$ molecules bound to subsites +1 to +4, while the other bound to subsites −1 to −4. Individual sugar residues bound in a linear conformation with the chair configuration for all sugar residues. However, the glycosidic linkage between −2 and −3 GlcNAcs appears to be twisted.

We compared the main chain conformation of RSC-c-E67Q/W72A liganded with $2 \times (GlcNAc)_4$ to those of unliganded RSC-c (PDB code: 4DWX) and RSC-c liganded with $(GlcNAc)_4$ (PDB code: 4DYG), in which only one $(GlcNAc)_4$ molecule bound to subsites +1 to +4 [18]. As shown in Fig. 2A, the main chain conformation of the

RSC-c-E67Q/W72A liganded with $2 \times (GlcNAc)_4$ (orange) was similar to that of unliganded RSC-c (black). Upon binding of $2 \times (GlcNAc)_4$, however, the pointed end of Loop III moved toward inside by 3.9 Å, and those of Loops IV and V moved inside by 1.6 and 1.4 Å, respectively. Nomenclatures of the loop structures are based on the report by Taira et al. [11]. The conformations of the hinge region almost overlapped each other. The shifts of the loop structures were also observed between RSC-c-E67Q/W72A liganded with $2 \times (GlcNAc)_4$ and RSC-c liganded with $(GlcNAc)_4$ (Fig. 2B). The individual loops similarly moved inside upon $(GlcNAc)_4$ binding to the negatively numbered subsites. The shifts of the pointed ends of the loop structures III, IV, and V were 3.5, 2.2, and 1.8 Å, respectively. On the other hand, comparison between RSC-c liganded with $(GlcNAc)_4$ and unliganded RSC-c exhibited only small shifts in the loop structures (Fig. 2C). The shifts of the loops were below 0.3 Å. Thus, domain motion was most likely to take place upon the oligosaccharide binding to the negatively numbered subsites which tightly cramp the oligosaccharide chains. Oligosaccharide binding to the positively numbered subsites did not bring about such a domain motion. It is likely that the domain motion is related to the catalytic mechanism, which will be discussed below.

3.2. $(GlcNAc)_4$ binding mode to subsites +1 to +4

The mode of $(GlcNAc)_4$ binding to subsites +1 to +4 was partly similar to that observed in the crystal structure reported for RSC-c liganded with $(GlcNAc)_4$ [18]; however, some interactions were rearranged in RSC-c-E67Q/W72A liganded with $2 \times (GlcNAc)_4$, as shown in Fig. 3. The hydroxyl on C-3 of +1 GlcNAc (the sugar occupying the +1 subsite) forms a hydrogen bond with the Oε atom of Gln118, which further interacts with the N2 atom of the *N*-acetyl group of +1 GlcNAc. The O7 atom of the *N*-acetyl group of +1 GlcNAc is also recognized by a hydrogen bond with the main chain nitrogen of Arg90. On the other hand, the hydroxyl on C-6 of +1 GlcNAc strongly interacts with Oε of Glu203, Nη of Arg215, and Nε of His66. The hydroxyl on C-6 of +2 GlcNAc provides a hydrogen bond to the main chain carbonyl of Thr69, which in turn accepts a hydrogen bond from the hydroxyl on C-3 of +3 GlcNAc. The *N*-acetyl group of +3 GlcNAc is recognized through a hydrogen bond between the N2 atom of the *N*-acetyl group and the main chain carbonyl of Gly70. The O7 atom of the *N*-acetyl group of +3 GlcNAc also makes a hydrogen bond with the side chain of Arg90. As reported previously for RSC-c liganded with $(GlcNAc)_4$, Trp72 of RSC-c was shown to be involved in a face-to-face stacking interaction with the +4 sugar [18]. In this study, however, Trp72 was mutated to alanine, and the stacking interaction was removed at this subsite. Instead, a water-mediated hydrogen bond was formed between Oγ of Thr74 and the +4 sugar. Removal of the stacking interaction of Trp72 did not significantly affect the location of the bound oligosaccharide. This might have been due to many hydrophobic and van der Waals interactions found in the lower part of the substrate binding cleft. In addition, the mutations of Glu67 and Trp72 rearranged the binding interactions at subsite +1, which resulted in the stronger recognition of GlcNAc at this subsite of RSC-c-E67Q/W72A. This situation did not change the location of the bound $(GlcNAc)_4$.

3.3. $(GlcNAc)_4$ binding mode to subsites −1 to −4

For −1 GlcNAc, direct hydrogen bonds are formed between the hydroxyl on C-1 and Oε of Glu89, the N2 atom of *N*-acetyl group and Oη of Tyr96, and the hydroxyl on C-6 and Nε of Gln67. A water-mediated hydrogen bond is also formed between O7 of the N-acetyl group and Nδ of Asn199. −2 GlcNAc is most strongly recognized by Ser120, His121, Asn124 (the N-terminal part of the helix α4), Ile198, and Gly201 (from the C-terminal of α9 to the N-terminal of α10). The O7 atom of the *N*-acetyl group is hydrogen-bonded with the main chain nitrogen and oxygen atoms of Ser120 and Nδ of Asn124. The pyranose-ring oxygen interacts with the Nε atom of His121. The N2 atom of the *N*-acetyl group directly interacts with the main chain oxygen of Ile198, and the hydroxyl of C-6 interacts with the Oδ of Asn199 and the main chain nitrogen of Gly201 by water-mediated hydrogen bonds. On the other hand, −3 and −4 GlcNAcs are weakly recognized by the enzyme. Two water-mediated hydrogen bonds are formed between the main chain

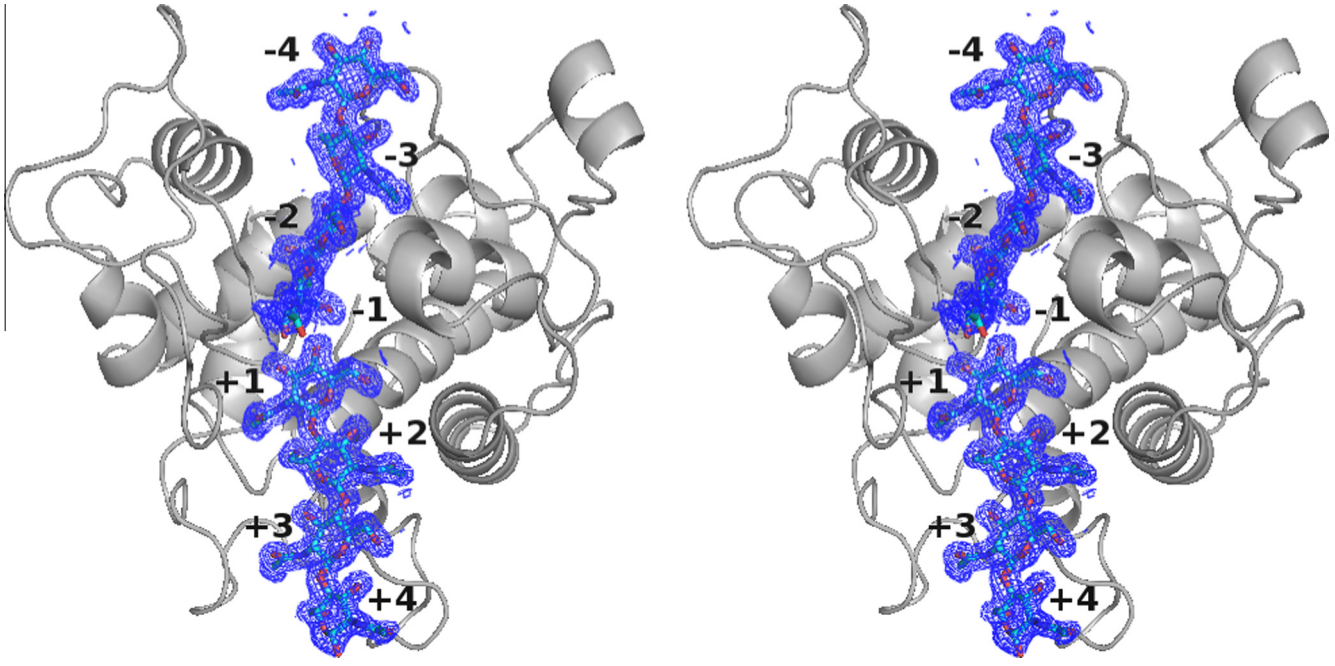

Fig. 1. Stereo view of simulated annealing-omit maps of the two molecules of $(GlcNAc)_4$ bound to RSC-c-E67Q/W72A. The map is colored in blue and contoured at 1.0 σ. The two $(GlcNAc)_4$ molecules are displayed by stick model colored in cyan. The individual subsites are numbered according to the subsite nomenclature proposed by Davies et al. [17].

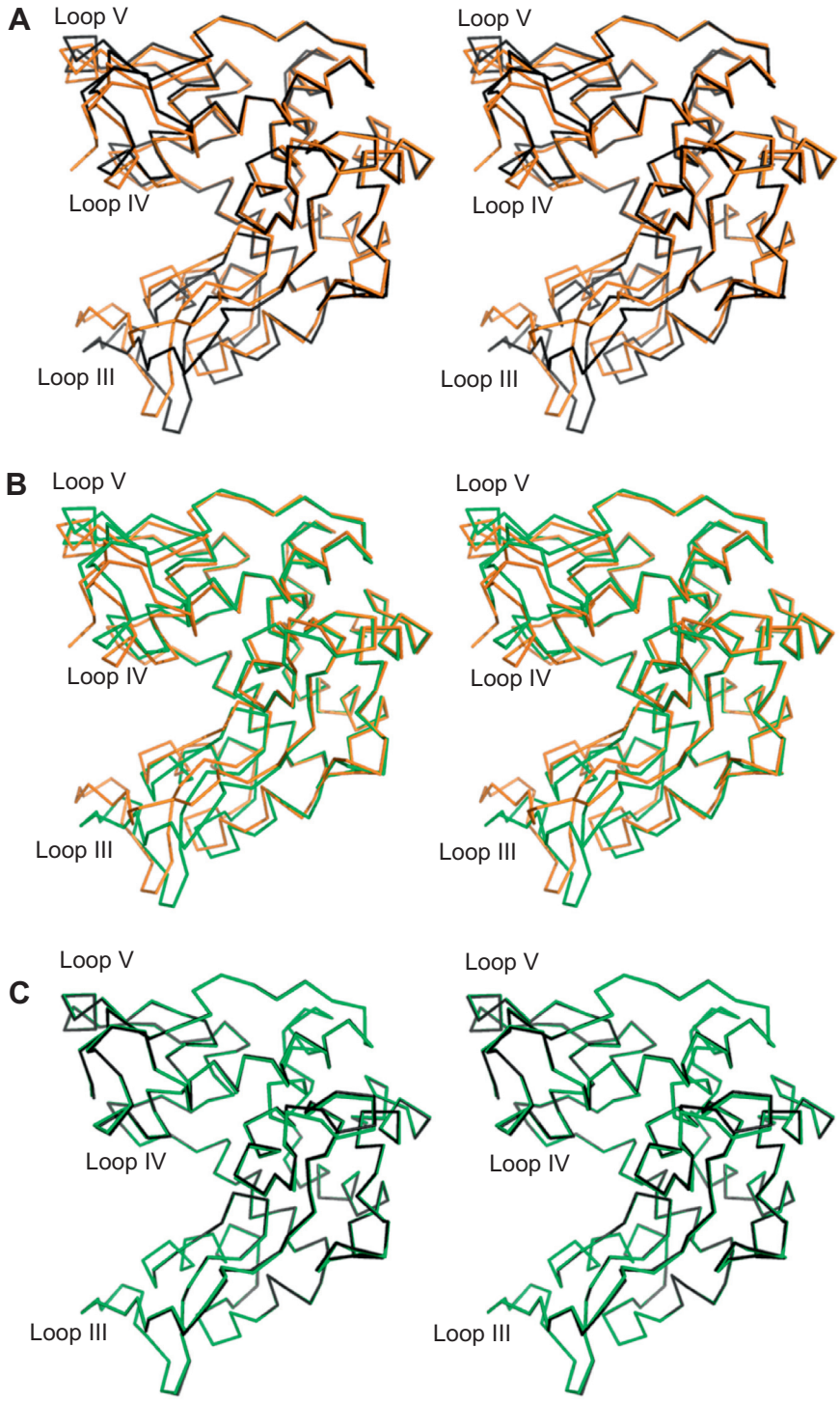

Fig. 2. Stereo views of superimpositions of the main chain structures of RSC-c-E67Q/W72A liganded with 2 × $(GlcNAc)_4$ and unliganded RSC-c (A), RSC-c-E67Q/W72A liganded with 2 × $(GlcNAc)_4$ and RSC-c liganded with $(GlcNAc)_4$ (B), and RSC-c liganded with $(GlcNAc)_4$ and unliganded RSC-c (C). The main chains are displayed with wire models colored in orange (RSC-c-E67Q/W72A liganded with 2 × $(GlcNAc)_4$), green (RSC-c liganded with $(GlcNAc)_4$; PDB code, 4DYG), and black (unliganded RSC-c; PDB code, 4DWX).

nitrogen of Phe242 and the O7 atom of the *N*-acetyl group of −3 GlcNAc and between the main chain oxygen of Phe242 and the hydroxyl on C-6 of −4 GlcNAc. Oε of Gln162 is also involved in the hydrogen bond with the hydroxyl on C-6 of the −3 sugar. Similar to that observed in the positively numbered subsites, many hydrophobic and van der Waals interactions are found in the negatively numbered subsites. Overall, the oligosaccharide binding to the negatively numbered subsites is dominated by the GlcNAc residue interaction at subsite −2. This is consistent with the binding free energy data reported for the individual subsites for "loopful" GH19 chitinases [15,16].

The binding model of $(GlcNAc)_6$ to the "loopful" GH19 chitinase from barley seeds was constructed by a molecular dynamics (MD) simulation [25] based on the crystal structure of the unliganded barley enzyme [26]. The amino acid sequence of the barley enzyme is 92% identical to that of RSC-c. In the binding model obtained from

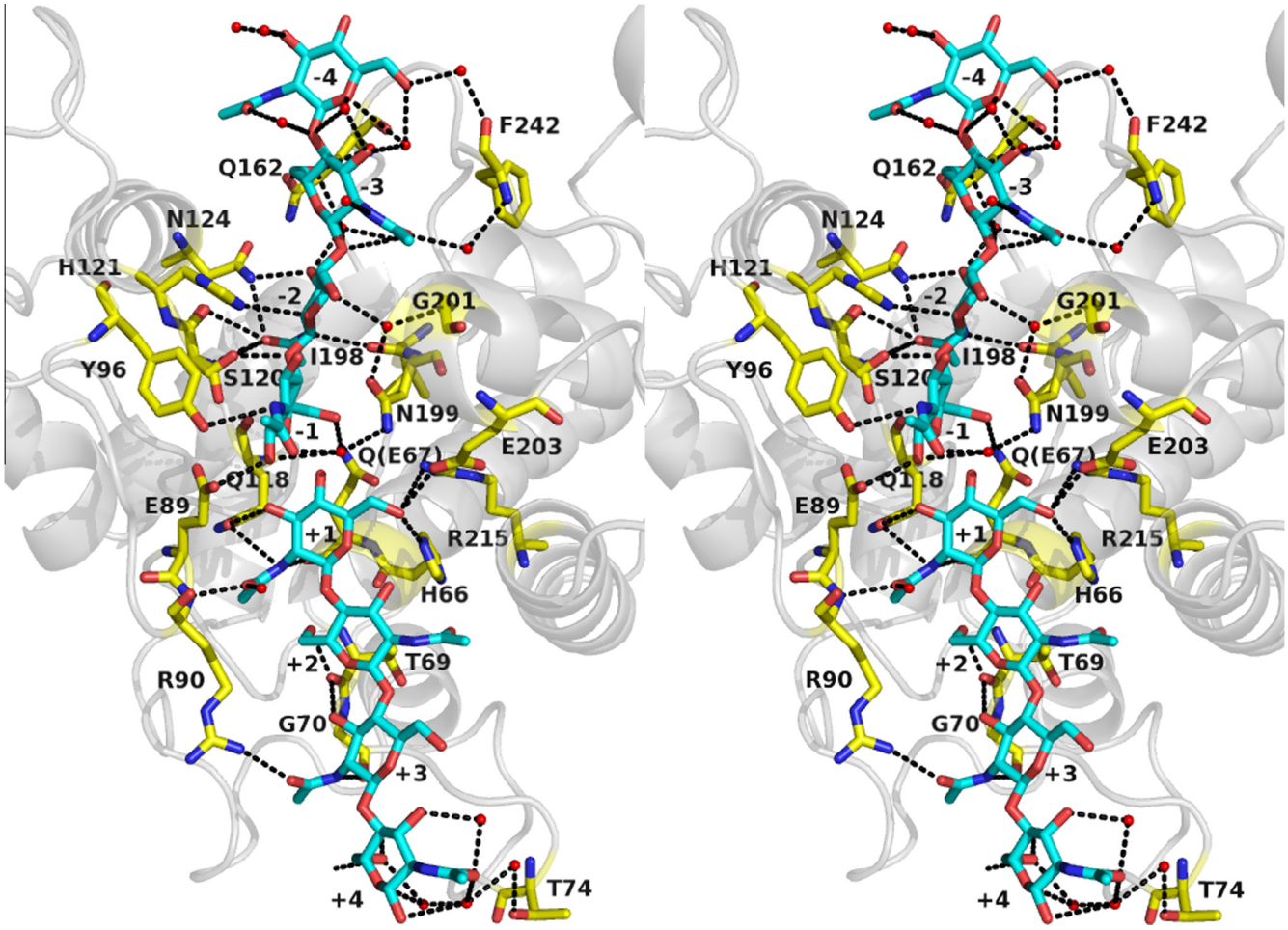

Fig. 3. Stereo view of the amino acid residues of RSC-c-E67Q/W72A interacting with two molecules of $(GlcNAc)_4$. The two $(GlcNAc)_4$ molecules are displayed by stick model colored in cyan. The amino acid residues interacting with the ligands are displayed by stick model colored in yellow. Hydrogen bonds are shown as dashed lines. The individual subsites are numbered as in Fig. 1.

MD, several amino acid residues located in the binding cleft were shown to be involved in the interaction with $(GlcNAc)_6$. These were Trp103 and Gln162 for −4 GlcNAc, Tyr123, Asn124, and Lys165 for −3 GlcNAc, Ile198, Ser120 and Asn124 for −2 GlcNAc, and Glu67 and Asn199 for −1 GlcNAc. All of these amino acids are completely conserved in RSC-c. The amino acid residues contributing to the interactions with −1 and −2 GlcNAcs are almost identical to those found in the crystal structure of RSC-c-E67Q/W72A liganded with $2 \times (GlcNAc)_4$ (Fig. 3). However, the amino acid residues interacting with −3 and −4 GlcNAcs are different from those observed in the crystal structure. The weak interactions at subsites −3 and −4 might have resulted in the flexibility of the bound sugars, which suggests several possibilities for the binding mode in MD calculations.

Huet et al. reported the modeled structure of a "loopful" GH19 chitinase from papaya, in which $(GlcNAc)_4$ bound to subsites −2 to +2 [10]. The amino acid residues involved in the interactions with −2 GlcNAc in the modeled structure, for example, Tyr123, Gln162, and Lys165, are markedly different from those observed in the crystal structure reported here. This might be due to the absence of GlcNAc residues at subsites −3 and −4.

3.4. Catalytic mechanism

The catalytic mechanism of GH19 chitinase was also proposed by an MD simulation [25]. Glu67 donates the proton to glycosyl oxygen to cleave the β-1,4-glycosidic linkage. This bond cleavage leads to the formation of an oxocarbenium ion intermediate, which undergoes a nucleophilic attack of the water molecule activated by the carboxylate of Glu89. The water molecule is coordinated by the hydroxyl of Ser120. A similar mechanism has also been proposed by Huet et al. [10], and is basically supported by the crystal structure reported here. Fig. 4 shows a close-up view of the catalytic center, in which the structures of RSC-c-E67Q/W72A liganded with $2 \times (GlcNAc)_4$ (orange) and unliganded RSC-c (black) are superimposed. It should be noted that the conformational change derived from the oligosaccharide binding to the negatively numbered subsites significantly narrows the distance between Glu67 and Glu89, resulting in effective stabilization of the oxocarbenium ion intermediate. This conformational change also narrows the distance between Glu67 and Ser120, which facilitates the nucleophilic attack of the water molecule coordinated by Ser120 to the C-1 of −1 GlcNAc. Thus, our crystallographic results provide experimental evidence that strongly supports the catalytic mechanism proposed by Brameld and Goddard III [25]. When the main chain of RSC-c-E67Q/W72A liganded with $2 \times (GlcNAc)_4$ was superimposed with that of papaya chitinase liganded with two GlcNAcs at −2 and + 1 [10], the deviations (an rmsd, 0.402 Å) were found at the ends of the loop structures, but not at the catalytic cleft including the residues Glu67, Glu89, and Ser120. Taken together, we conclude that conformational changes shown in Figs. 2A and

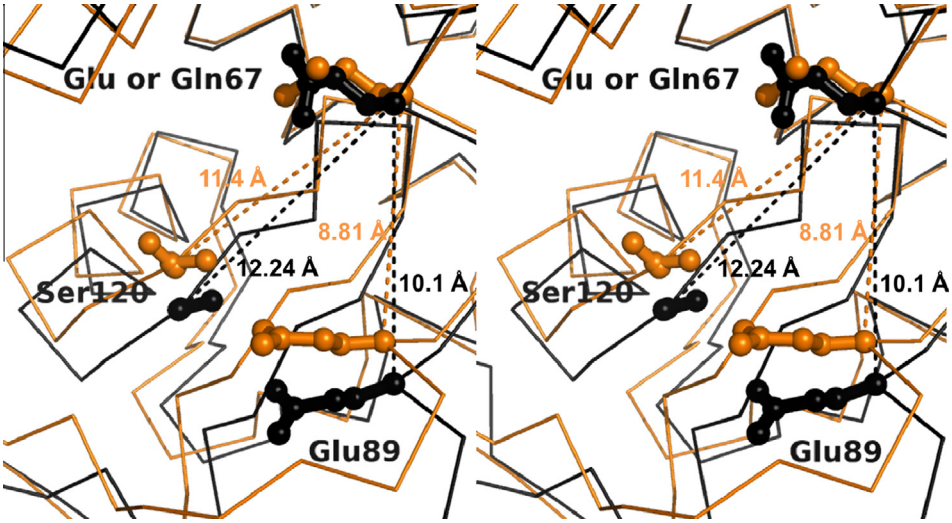

Fig. 4. Stereo view of the catalytic center. The structures of RSC-c-E67Q/W72A liganded with 2 × $(GlcNAc)_4$ (orange) and unliganded RSC-c (black) were superimposed. Glu67 acts as the proton donor, Glu89 activates the nucleophilicity of the water molecule, which is coordinated by the hydroxyl of Ser120. Dashed lines indicate the distances between the α-carbons of the corresponding residues.

B are resulting from the binding of oligosaccharide to the negatively numbered subsites and are essential for the catalytic mechanism.

The structure of the oligosaccharide bound to RSC-c-E67Q/W72A did not provide any information on the transition state, because −1 GlcNAc adopts a stable chair configuration (Fig. 3). It is highly desirable to obtain crystal structures capturing the transition state of −1 GlcNAc to obtain further details on the catalytic mechanism.

3.5. Conclusions

The "loopful" GH19 chitinase from rye seeds, RSC-c, can accommodate eight GlcNAc residues in the substrate-binding cleft. Among the eight subsites, the GlcNAc residues at +1, −1, and −2 are strongly recognized by the enzyme. Comparisons of the main chain conformation between RSC-c-E67Q/W72A liganded with 2 × $(GlcNAc)_4$ and unliganded RSC-c reveals domain motion upon oligosaccharide binding. This domain motion might be essential for chitin hydrolysis. These structural findings can be applied to the other "loopful" GH19 chitinases from plants because of their high sequence homology.

Acknowledgments

This work was supported by "Strategic Project to Support the Formation of Research Bases at Private Universities: Matching Fund Subsidy from MEXT (Ministry of Education, Culture, Sports, Science and Technology), 2011–2015 (S1101035).

Appendix A. Supplementary data

Supplementary data associated with this article can be found, in the online version, at http://dx.doi.org/10.1016/j.febslet.2013.07.008.

References

[1] Henrissat, B. and Davies, G.J. (1997) Structural and sequence-based classification of glycoside hydrolases. Curr. Opin. Struct. Biol. 7, 637–644.
[2] Fukamizo, T., Sato, H., Mizuhara, M., Ohnuma, T., Gotoh, T., Hiwatashi, K. and Takahashi, S. (2011) Chitinase from *Autographa californica* multiple nucleopolyhedrovirus: rapid purification from Sf-9 medium and mode of action. Biosci. Biotechnol. Biochem. 75, 1763–1769.
[3] Vaaje-Kolstad, G., Horn, S.J., Sørlie, M. and Eijsink, V.G. (2013) The chitinolytic machinery of Serratia marcescens – a model system for enzymatic degradation of recalcitrant polysaccharides. FEBS J. 280, 3028–3049.
[4] Hartl, L., Zach, S. and Seidl-Seiboth, V. (2012) Fungal chitinases: diversity, mechanistic properties and biotechnological potential. Appl. Microbiol. Biotechnol. 93, 533–543.
[5] Arakane, Y. and Muthukrishnan, S. (2010) Insect chitinase and chitinase-like proteins. Cell. Mol. Life Sci. 67, 201–216.
[6] Bleau, G., Massicotte, F., Merlen, Y. and Boisvert, C. (1999) Mammalian chitinase-like proteins. in Chitin and Chitinases. EXS 87, 211–221.
[7] Arakane, Y., Taira, T., Ohnuma, T. and Fukamizo, T. (2012) Chitin-related enzymes in agro-biosciences. Curr. Drug Targets 13, 442–470.
[8] Takenaka, Y., Nakano, S., Tamoi, M., Sakuda, S. and Fukamizo, T. (2009) Chitinase gene expression in response to environmental stresses in *Arabidopsis thaliana*: chitinase inhibitor allosamidin enhances stress tolerance. Biosci. Biotechnol. Biochem. 73, 1066–10671.
[9] Hart, P.J., Monzingo, A.F., Ready, M.P., Ernst, S.R. and Robertus, J.D. (1993) Crystal structure of an endochitinase from *Hordeum vulgare* L. seeds. J. Mol. Biol. 229, 189–193.
[10] Huet, J., Rucktooa, P., Clantin, B., Azarkan, M., Looze, Y., Villeret, V. and Wintjens, R. (2008) X-ray structure of papaya chitinase reveals the substrate binding mode of glycosyl hydrolase family 19 chitinases. Biochemistry 47, 8283–8291.
[11] Taira, T., Mahoe, Y., Kawamoto, N., Onaga, S., Iwasaki, H., Ohnuma, T. and Fukamizo, T. (2011) Cloning and characterization of a small family 19 chitinase from moss (*Bryum coronatum*). Glycobiology 21, 644–654.
[12] Kezuka, Y., Ohishi, M., Itoh, Y., Watanabe, J., Mitsutomi, M., Watanabe, T. and Nonaka, T. (2006) Structural studies of a two-domain chitinase from *Streptomyces griseus* HUT6037. J. Mol. Biol. 358, 472–484.
[13] Hoell, I.A., Dalhus, B., Heggset, E.B., Aspmo, S.I. and Eijsink, V.G. (2006) Crystal structure and enzymatic properties of a bacterial family 19 chitinase reveal differences from plant enzymes. FEBS J. 273, 4889–4900.
[14] Ubhayasekera, W., Rawat, R., Ho, S.W., Wiweger, M., von Arnold, S., Chye, M.L. and Mowbray, S.L. (2009) The first crystal structures of a family 19 class IV chitinase: the enzyme from Norway spruce. Plant Mol. Biol. 71, 277–289.
[15] Honda, Y. and Fukamizo, T. (1998) Substrate binding subsites of chitinase from barley seeds and lysozyme from goose egg white. Biochim. Biophys. Acta 1388, 53–65.
[16] Sasaki, C., Itoh, Y., Takehara, H., Kuhara, S. and Fukamizo, T. (2003) Family 19 chitinase from rice (*Oryza sativa* L.): substrate-binding subsites demonstrated by kinetic and molecular modeling studies. Plant Mol. Biol. 52, 43–52.
[17] Davies, G.J., Wilson, K.S. and Henrissat, B. (1997) Nomenclature for sugar-binding subsites in glycosyl hydrolases. Biochem. J. 321, 557–559.
[18] Ohnuma, T., Numata, T., Osawa, T., Inanaga, H., Okazaki, Y., Shinya, S., Kondo, K., Fukuda, T. and Fukamizo, T. (2012) Crystal structure and chitin oligosaccharide-binding mode of a 'loopful' family GH19 chitinase from rye, *Secale cereale*, seeds. FEBS J. 279, 3639–3651.
[19] Ohnuma, T., Yagi, M., Yamagami, T., Taira, T., Aso, Y. and Ishiguro, M. (2002) Molecular cloning, functional expression, and mutagenesis of cDNA encoding

rye (*Secale cereale*) seed chitinase-c. Biosci. Biotechnol. Biochem. 66, 277–284.
[20] Otwinowski, Z. and Minor, W. (1997) Processing of X-ray diffraction data collected in oscillation mode. Methods Enzymol. 276, 307–326.
[21] Vagin, A. and Teplyakov, A. (1997) MOLREP. An automated program for molecular replacement. J. Appl. Crystallogr. 30, 1022–1025.
[22] Murshudov, G.N., Vagin, A.A. and Dodson, E.J. (1997) Refinement of macromolecular structures by the maximum-likelihood method. Acta Crystallogr. D Biol. Crystallogr. 53, 240–255.
[23] Emsley, P. and Cowtan, K. (2004) Coot. Model-building tools for molecular graphics. Acta Crystallogr. D Biol. Crystallogr. 60, 2126–2132.
[24] Laskowski, R.A., MacArthur, M.W., Moss, D.S. and Thornton, J.M. (1993) PROCHECK. A program to check the stereochemical quality of protein structures. J. Appl. Crystallogr. 26, 283–291.
[25] Brameld, K.A. and Goddard III, W.A. (1998) The role of enzyme distortion in the single displacement mechanism of family 19 chitinases. Proc. Natl. Acad. Sci. USA 95, 4276–4281.
[26] Hart, P.J., Pfluger, H.D., Monzingo, A.F., Hollis, T. and Robertus, J.D. (1995) The refined crystal structure of an endochitinase from *Hordeum vulgare* L. seeds at 1.8 Å resolution. J. Mol. Biol. 248, 402–413.